**1. Marek PISZCZEK, 2. Aleksandra KUCHARCZYK-DRAB, 3. Adam PISZCZEK**

ORCID: 1. 0000-0003-3376-6427; 2. 0000-0002-3821-5918; 3. 0009-0000-6477-6017

OPEN ACCESS

**DOI: 10.15199/48.2025.05.47**

# ArduCam vision sensors for cosmic-ray detection and analysis

*Zastosowanie czujników wizyjnych ArduCam do wykrywania i analizy promieniowania kosmicznego*

***Abstract**. The study of secondary cosmic radiation can be implemented with the help of relatively simple components that are vision sensors capable of recording the traces of impacts left on images. The article presents the elements of the implemented concept of IoT system, one of the important elements of which is to be vision sensors. The main part of the article pays attention to the selection of operating parameters of such sensors from the point of view of efficient acquisition and detection of potential traces and their analysis including elements of classification.*

***Streszczenie.** Badania dotyczące wtórnego promieniowania kosmicznego można realizować za pomocą względnie prostych komponentów jakimi są sensory wizyjne zdolne rejestrować pozostawione na obrazach ślady oddziaływań. W artykule przedstawiono elementy realizowanej koncepcji systemu IoT, której jednym z istotnych elementów mają być czujniki wizyjne. Główna część artykułu zwraca uwagę na dobór parametrów pracy takich czujników z punktu widzenia efektywnej akwizycji i wykrywania potencjalnych śladów oraz ich analizy łącznie z elementami klasyfikacji.*

**Keywords:** cosmic-ray, vision sensor, edge computing, IoT
**Słowa kluczowe:** promieniowanie kosmiczne, czujnik wizyjny, przetwarzanie brzegowe, IoT

## Introduction

Cosmic rays, originating from the farthest reaches of the Universe, constitute one of the most fascinating astrophysical phenomena. When high-energy cosmic particles penetrate the Earth's atmosphere, they initiate a process known as an air shower (Fig. 1). This phenomenon is created by the interaction of a primary particle, such as a proton, atomic nucleus, or photon, with atmospheric particles, resulting in the production of a cascade of secondary particles.

Pierre Auger was a pioneer in the study of cosmic-ray detection and observation, providing the first evidence of extensive air showers in the 1930s [1]. Through experimental investigations, Auger demonstrated the synchronous detection of particles across detectors separated by significant distances, attributing these observations to the interaction of high-energy primary particles with the atmosphere, which initiates cascades of secondary particles. Over two decades later, Greisen mathematically predicted the expected flux of muons at the Earth's surface, further advancing the theoretical understanding of these phenomena [2]. These foundational studies has led to the development of large-scale observatories worldwide, including the Pierre Auger Observatory [3], the Large High Altitude Air Shower Observatory [4], and the Telescope Array [5-6], which continue to refine our understanding of cosmic-ray interactions and their underlying mechanisms.

The results of contemporary research allow scientists to determine approximately what particle intensity can be expected [7]. Statistical analyses estimate this flux at approximately ~1/cm²/min. The angular distribution of muons at the surface can be modelled by the relationship $\cos^2\theta$, characteristic of particles with energies around 3 GeV. At lower energies, the angular distribution broadens, extending to angles as large as 90°. Given the extensive nature of particle showers reaching the Earth's surface, their detection requires coverage over a large area rather than localized, point-based measurements. Based on the spatial distribution of secondary particles and the observed frequency of these phenomena, the campus of the Military University of Technology has been identified as a suitable location for conducting such investigations (Fig. 1).

The research being carried out on atmospheric bursts is aimed at new phenomena such as dark matter, the presence of which can be detected indirectly by affecting cosmic ray particles. Furthermore, muon detection techniques are used in particle acceleration experiments in laboratories and in environmental radiation monitoring.

In the context of astronomy, measurements of atmospheric bursts contribute to the discovery of new sources of high-energy radiation, such as pulsars or supernovae.

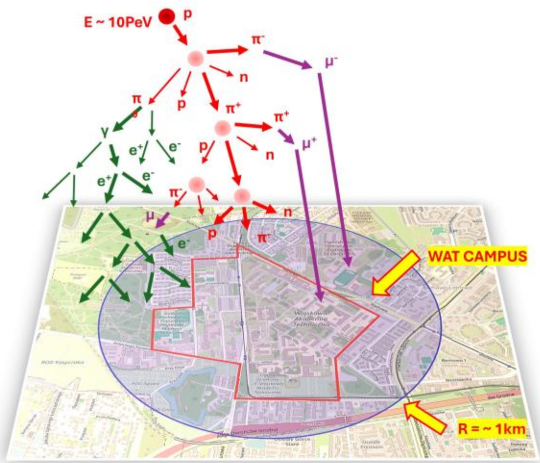


Fig. 1. Visualization of air shower.

The paper presents the concept of cosmic ray detection using IoT technology, including an overview of the available test instruments. Subsequent chapters include a characterisation of the parameters of the vision sensors used in the experiments and an analysis of the properties of the sensors with their comparison. The radiation detection algorithms implemented in the developed system are also described. The final sections of the paper present the results of the analysis of the recorded radiation and supporting solutions, such as dedicated tools for IoT system management and integration with the CREDO database.

## Concept of measurements system based on IoT sensors

Current research on cosmic rays is focused on several key areas, including the reconstruction of air shower profiles using optical telescope networks to capture phenomena such as Cherenkov radiation, the determination of the energy and trajectory of incoming cosmic rays, and the detection of temporal coincidences of particles arriving at the Earth's surface using distributed detector networks [8-

11]. Given the characteristics of cosmic-ray interactions with the atmosphere, studies of primary cosmic radiation are typically conducted in space [12] or at high altitudes using balloon-borne instruments [13], as only a small fraction of primary particles reach the Earth's surface. The ground-based hardware is primarily dedicated to the detection of secondary cosmic radiation, using a variety of measurement systems: bubble chambers, scintillation counters as well as semiconductor detectors including vision matrix detectors 2D.

In addition to high-budget, large-scale scientific initiatives, research on cosmic radiation is also pursued through "citizen science" projects, which serve both to advance scientific understanding and to promote public engagement. Notable examples include "DECO" [14] and "CREDO" [15], which focus on detecting and analyzing the geometries of tracks formed in images captured by matrix sensors as a result of ionization in semiconductor materials. Other projects, such as "cosmicπ" [16] and "CosmicWatch" [17], emphasize particle counting combined with precise time measurements, leveraging scintillations generated in crystals through interactions with secondary cosmic radiation.

The proposed IoT-based system for the investigation of secondary cosmic radiation integrates multiple types of sensors designed for specific tasks, including track detection and precise event timing. The solutions described in this study are currently funded by a group of enthusiasts, and the associated resource constraints necessitate the adoption and implementation of innovative low-cost methodologies. Muon detection sensors provide highly accurate timestamps corresponding to the formation of air showers, which are transmitted to a central server for synchronization with data from vision sensors. By buffering images, these sensors can retransmit images according to a timestamp and then reset the memory to that point. This hybrid system design reduces hardware resource demands, increases the number of detectable phenomena, and significantly improves the temporal resolution of measurements (Fig. 2).

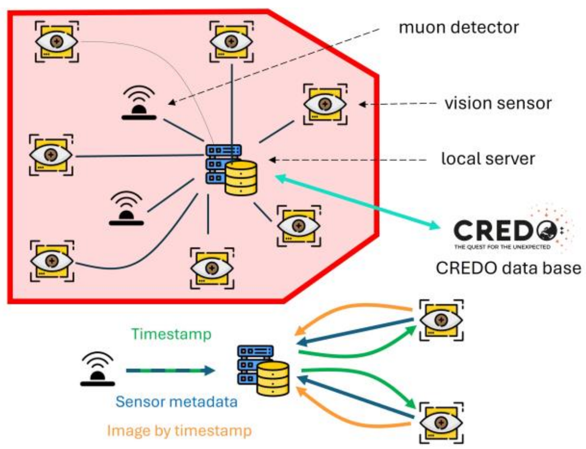


Fig. 2. General structure and basic functionality of IoT vision sensor-based measurement system.

**Vision sensor**

The focus of the current work on the IoT system characterised above is on optimising the hardware and software configurations of the vision sensor (Fig. 3). To date, evaluations have been conducted using various Raspberry Pi controllers (Zero, 3B, 4B, 5) and vision sensors. This article narrows its focus to the most promising configurations, presenting results for the Raspberry Pi 4B and 5 models. The findings are based on five widely used sensors, four of which operated in rolling-shutter mode (OV5647, IMX219, IMX477, HawkEye), and one with global shutter mode (IMX296).

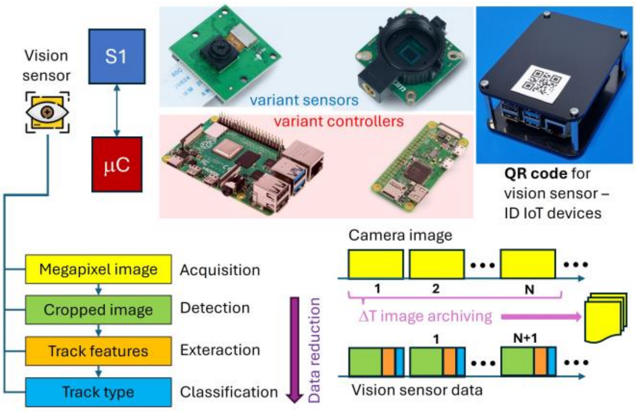


Fig. 3. Vision sensor - configuration and operation.

For the sensors operation configuration used, due to the much higher averaged noise level of the OV5647 sensor (>20 units) relative to the other models (<1) and also its operational instability observed in conjunction with the Raspberry Pi 5, the majority of the results presented focus on the remaining four sensor types. The key parameters of these sensors are presented in Table 1.

Table 1. Popular sensors used in the tests

| Sensor type | Pixel size [μm] | Resolution [pix] |
|---|---|---|
| IMX296 | 3.45 | 1456 × 1088 |
| OV5647 | 1.4 | 2592 × 1944 |
| IMX219 | 1.12 | 3280 × 2464 |
| IMX477 | 1.55 | 4056 × 3040 |
| HawkEye | 0.8 | 9152 × 6944 |

The matrix-based vision sensor captures images that, even when acquired at 8-bit grayscale depth, occupy significant memory space in RAM or on disk during archival, due to the high native resolution. However, the primary function of the vision sensor within the IoT system is not the transmission of raw image data but the provision of processed and data-reduced information derived from frame-by-frame analysis. Similar to the approach adopted in the CREDO project, the sensor performs preliminary processing by detecting and cropping regions of interest (60x60 pixels) within the original image that may contain traces of cosmic radiation. This initial step achieves significant data reduction; for example, images from the HawkEye sensor, initially several megabytes in size, can be reduced to a few hundred bytes.

Subsequent analysis of these regions can enable metrological evaluation or content classification, further compressing data volumes to only a few bytes (e.g., classifying anomaly type, confirming potential muon detection, or estimating muon trajectory). The processing methods implemented in the developed vision sensor systems adhere to edge-computing principles, where data is processed locally at the sensor level. This approach facilitates the near real-time comparative analysis of processed traces with those recorded by other vision sensors.

The integration of the vision sensor within the IoT system is designed to ensure interoperability with other sensor types. Additionally, the vision sensor includes a functionality for buffering raw images within a narrow temporal window ΔT preceding the current acquisition. This enables the retrieval of "historical" images, guided by timestamp data from muon detectors, for further post-processing analysis on a central server.

**Cosmic-ray detection**

The fundamental component of a vision sensor is the matrix sensor, which converts the energy of incoming particles into electrical signals, enabling precise measurement and detailed analysis.

Semiconductor matrices are currently the most commonly used technology for the detection of secondary cosmic radiation. Examples include cadmium telluride (CdTe) and cadmium zinc telluride (CdZnTe) sensors [19], which are adept at detecting high-energy photons and particles while offering excellent energy resolution; silicon strip detectors, recognized for their high spatial resolution [20]; and CMOS sensors, which are ubiquitous in digital cameras and smartphones. Specific physical mechanisms responsible for trace formation on CMOS sensors include ionization, atomic displacement, charge accumulation, and charge leakage [21-22].

The relatively low cost of CMOS sensors has attracted considerable interest from the scientific community, leading to their incorporation into cosmic radiation research. These sensors have gained prominence due to the development of global detection networks utilizing smartphones equipped with CMOS technology. At the same time, this solution demonstrates the potential of a distributed sensing network and also highlights the possibility of using consumer electronics to collect valuable scientific data.

Secondary cosmic radiation interacting with CMOS sensors can generate distinctive traces due to the interaction of high-energy particles with the silicon substrate of the sensor. These traces commonly appear as artifacts on recorded images, manifesting as dots, lines, or irregular patterns (referred to colloquially as "worms"). A key challenge is the ability to distinguish these traces from other phenomena inherent to the operation of CMOS sensors, particularly under conditions of complete light isolation (e.g., with the camera lens obscured). This mode of operation is a prerequisite for the use of the sensors under consideration as cosmic ray detectors. However, it is not sufficient for their effective use in terms of data acquisition and, above all, data analysis. For this purpose, it is required to determine the specific operating parameters of such sensors, which will depend, among other things, on their noise properties and the occurrence of abnormal pixels. These parameters are essential for optimizing the performance of CMOS sensors in cosmic-ray detection and ensuring accurate and reliable data analysis.

The procedure for determining operational parameters involves identifying statistical anomalies or patterns in pixel intensity. This step is crucial due to the high degree of similarity between sensor-inherent phenomena and potential traces left by cosmic radiation in recorded images. Such anomalies, often unique to individual sensor matrices, commonly manifest as follows: hot pixels with abnormally high intensity in the absence of a light stimulus, cold pixels with abnormally low intensity, and dead or blocked pixels that exhibit a constant intensity value with no variation across multiple image frames.

In addition to detecting these anomalous pixels and regions of potential halo effects-often observed near the edges of the detection matrix-it is essential to characterize the spatial and temporal noise patterns associated with the sensor's operation. To mitigate noise-related effects, the automatic gain control of the vision sensors was disabled, and images were captured with a fixed ISO setting of 100. A visualization of the most significant and frequently observed undesirable effects accompanying cosmic-ray detection with CMOS sensors is shown in Fig. 4. Testing of the ArduCam sensor series demonstrated considerable variability in both the average noise levels and the number and intensity variation of hot pixels (Fig. 5).

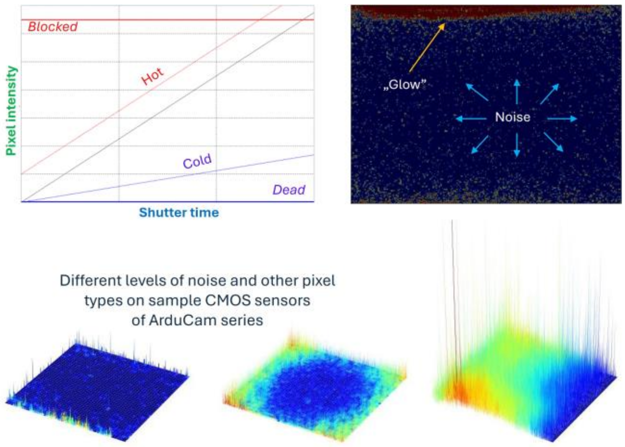


Fig. 4. Specific properties of the pixels of the CMOS sensor.

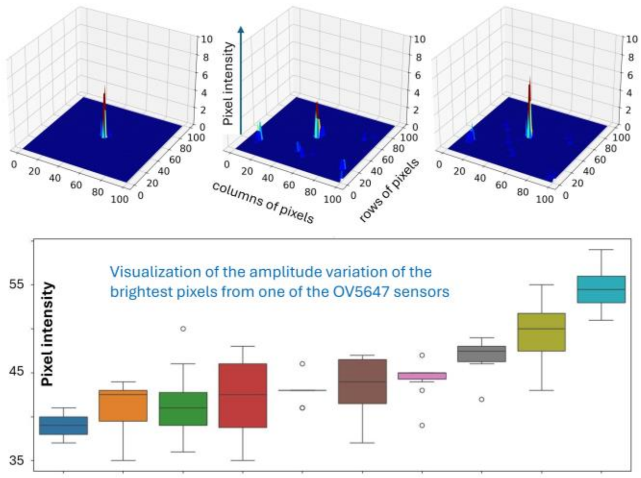


Fig. 5. 3D visualization and statistical analysis of anomalous pixels.

The sensor properties described above (excluding the temporal aspects of image analysis, which are discussed later in this article) is relevance in defining the operational parameters of vision sensors.

To establish a general framework for evaluating sensors for their suitability in cosmic-ray detection, four sensor types were tested, with three units of each type examined. The proposed methodology emphasizes two key objectives: maximizing the active detection time for cosmic radiation and minimizing the pixel intensity threshold used to analyze radiation-induced traces on images. These principles informed the optimization of all other aspects of vision sensor operation.

A fundamental component of the methodology involves determining the average pixel intensity, excluding outlier values. The results of these tests, conducted across various shutter speeds, are presented in Fig. 6. The results indicate that the selected sensors exhibit low spatially averaged noise levels across the matrix, supporting their potential as suitable candidates for vision-based cosmic-ray detection. Furthermore, the tests revealed relatively minor variability among individual units of the same sensor type, suggesting that the results are broadly representative of the tested sensor models.

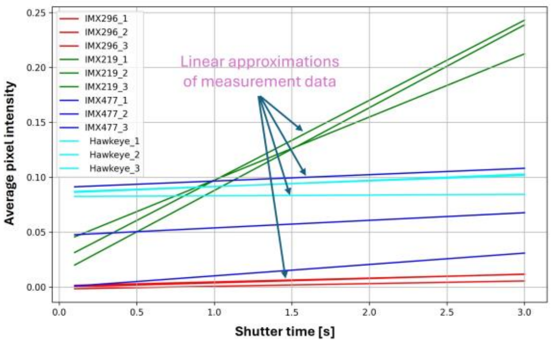


Fig. 6. Results of analysis of average pixel intensity in images recorded for different units of four sensor types.

Although the average noise levels are low, a significant challenge arises from the presence of hot pixels, which are the predominant issue. As shown in Fig. 7, there is substantial variability in both the number and amplitude of these pixels (independent of matrix size). This variability prevents the reduction of the detection and analysis threshold for pixel intensities to near-unity levels, as might be suggested by the average noise values. The reason for this is precisely the presence of anomalous pixels, the number of which would represent a large time burden for image analysis. In addition, these pixels would only represent measurement noise (artefacts) from the point of view of cosmic ray detection.

One of possible solution involves raising the analysis threshold above the level of hot pixels. However, this approach significantly reduced the ability to detect low-intensity traces formed on the sensor. An alternative strategy is to identify and manage these anomalous pixels at the analytical level. This latter approach has been implemented in the vision sensors discussed in this paper.

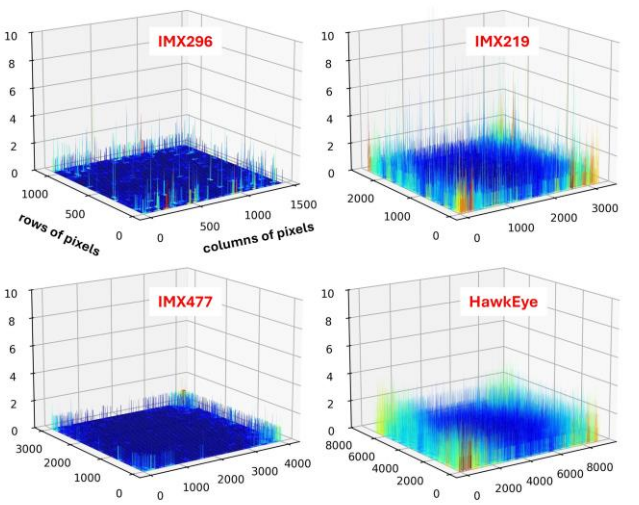


Fig. 7. Visualizations of average pixel intensity and abnormal pixels for different sensor types.

Each sensor is characterized by a unique distribution of anomalous pixels across its matrix, forming a distinct "fingerprint" that allows it to be differentiated from other devices (Fig. 8). This characteristic distribution can be utilized to enhance the detection rate of secondary cosmic-ray traces by enabling a controlled reduction in the pixel intensity detection threshold during image analysis.

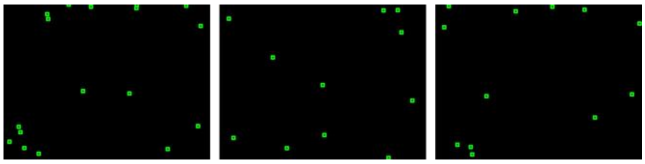

Fig. 8. Characteristic fingerprint of abnormal pixels on different units of the IMX296 type sensor

For cases where the number of pixels exceeding the detection threshold is relatively small, these regions can be filtered analytically. However, as the number of such pixels increases, it may become necessary to either acquire images with shorter detection times or compensate by raising the detection threshold. The acquisition time and detection threshold, which influence noise levels and the number of anomalous pixels (including the method for mapping recurrent pixels), represent critical parameters that define the operational performance of the vision sensor.

The distinct distribution of anomalous pixels for each sensor unit necessitates an individualized calibration approach. To quantify the number of pixels exceeding the detection threshold under varying conditions, a series of measurements was performed across different shutter times. These experiments were conducted for each sensor type, with shutter times ranging from 0.1 to 2.0 seconds (Fig. 9). For experimentally acceptable pixel counts in the range of 10–100, the pixel intensity threshold can be reduced to 5–15 for different sensor types, provided the sensor's shutter time does not exceed 500 ms.

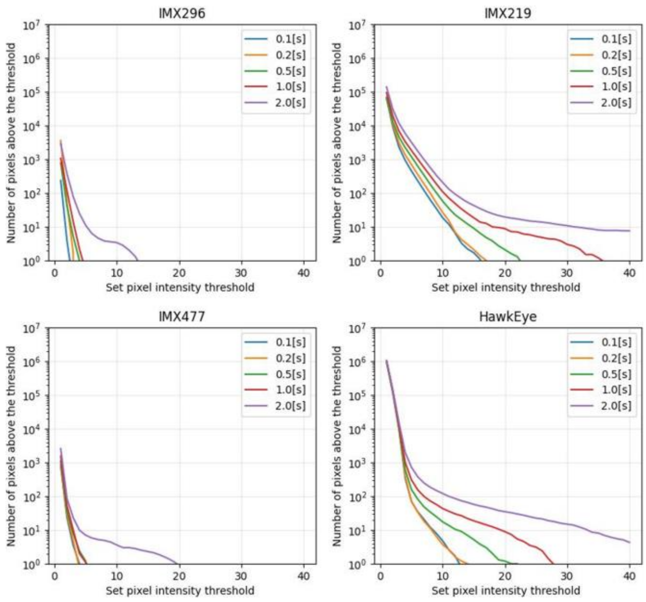


Fig. 9. Variability distributions of the number of suprathreshold pixels as a function of detection threshold and shutter speeds.

The use of extended shutter times may appear suboptimal from the perspective of temporal resolution for trace detection. However, the vision sensor cannot be regarded as a detector capable of delivering precise temporal data to the system. For phenomena of this nature occurring at relativistic speeds and the specified analysis area (approximately 1 km in radius), achieving directional estimates of cosmic radiation would require temporal data with a resolution of <1 μs.

Considering the computational demands and thermal effects associated with sensor operation, longer shutter times are essential to ensure sufficient time for processing each captured frame before acquiring the next. A vision sensor designed for cosmic radiation detection must not only perform image acquisition but also execute detailed image analysis at the required level of precision.

To evaluate these operational requirements, a study was conducted to assess the processing time associated with each stage of the sensor's algorithm. The experiments utilized vision sensors configured with various sensor types and two Raspberry Pi controllers (versions 4B and 5), both equipped with 8 GB of RAM. The developed algorithm (Fig. 10) identifies seven key points for measuring processing time (T1–T7).

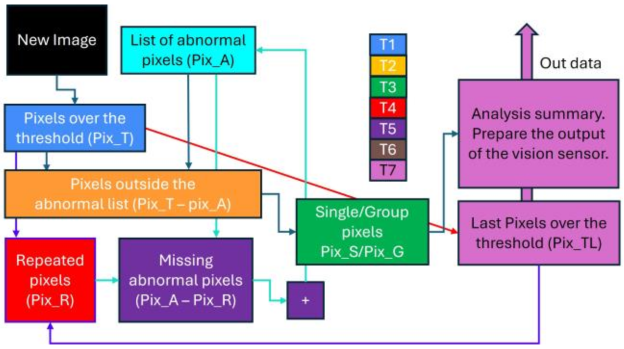


Fig. 10. Key elements of the vision sensor operating algorithm

Figures 11 and 12 present the statistical analysis of processing times recorded during normal operation of the vision sensors.

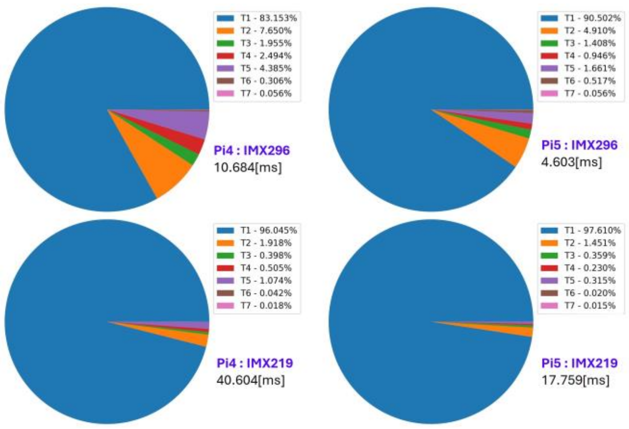


Fig. 11. Summary results of the analysis of the execution times of the various steps of the algorithm for IMX296 and IMX219.

To ensure consistency for comparative purposes, the same algorithm was implemented across all devices, utilizing a dedicated thread for image acquisition and a separate thread for image analysis. All sensors were configured with a uniform shutter time of 500 ms, while different pixel intensity thresholds were applied to maintain an approximately consistent number of above-threshold pixels requiring analysis. The image acquisition algorithm was developed using the *picamera2* library.

The Raspberry Pi 5 achieved nearly 100% active sensor runtime for all sensors while the Raspberry Pi 4B reach approximately 50% but in the HawkEye the efficiency was less than 25%. The findings indicate that the most computationally intensive stage is the initial phase, which involves generating a list of pixel indices with intensities exceeding the defined threshold. To optimize computational efficiency across the algorithm, this stage transitions from a 2D to a 1D data representation.

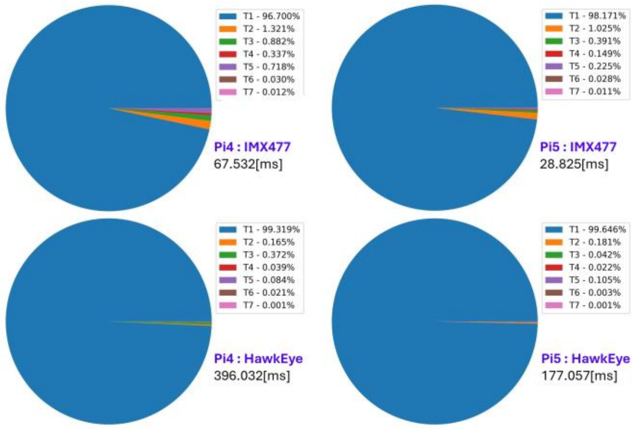


Fig. 12. Summary results of the analysis of the execution times of the various steps of the algorithm for IMX477 and HawkEye.

The results unequivocally demonstrate the superior performance of the Raspberry Pi 5 controller, achieving total analysis times that are more than twice as fast compared to other configurations. Additionally, the data reveal a clear correlation between sensor size and total analysis time.

In the proposed baseline algorithm, the vision sensor conducts fundamental image analysis, incorporating a classification thread to distinguish between point-like and group-like objects. The information extracted regarding the geometric arrangement of pixels within the cropped image fragment (60x60 pixels) is essential for subsequent analyses, particularly for identifying characteristic cosmic-ray traces.

The measurement results indicate that the time allocated for image content analysis does not represent a significant computational burden. Consequently, depending on the sensor type and the data analysis controller used, more advanced analytical functionalities can be implemented. These may include enhanced object classification or metrological assessments, further expanding the analytical potential of the system.

**Elements of edge computing in system IoT**

Edge computing represents a distributed data processing paradigm that relocates computation and data storage closer to the sources of data acquisition. In the proposed IoT system, this functionality is carried out by vision sensors, which perform a substantial portion of the computations and deliver highly processed data to the server. Additionally, the sensors possess the capability to temporarily store limited image datasets and transmit them to the server for advanced processing when required.

Although the computational capabilities of the vision sensors are less advanced than those of the server, they can effectively perform essential tasks such as image pre-processing, statistical and geometric analyses, and basic object recognition. This approach not only enhances the system’s efficiency by distributing computational loads but also facilitates localized data processing, reducing latency and enabling faster initial analyses.

As part of testing various algorithms implemented on Raspberry Pi 5 for distinguishing detected traces in images, methods incorporating machine learning were investigated. One such approach focused on the characterization and classification of cosmic-ray traces through geometric analysis, enabling the identification, isolation, and measurement of features associated with specific shapes, such as "dots," "lines," and "worms”.

Using binarized images (generated based on a predefined pixel intensity threshold), morphological operations such as opening, closing, and skeletonization were applied. These steps facilitated the analysis and quantification of shape-specific features, including area, perimeter, aspect ratio, and convexity. In subsequent steps (edge processing of the data) using the above-mentioned features, a classifier, e.g. Random Forest, can be trained, allowing (with limited accuracy) the determination of 3 characteristic types of traces (Fig. 13) This solution at the same time is an extension of the baseline classification with the division into point and group objects while acceptably increasing computation time.

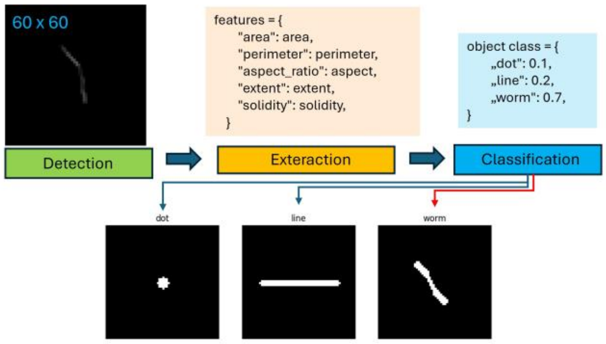


Fig. 13. Classification using Random Forest

Single-board computers, such as those in the Raspberry Pi family, provide a cost-effective, energy-efficient platform with support for hardware accelerators, making them suitable for the implementation of neural networks. These systems enable processing either through dedicated AI modules or cameras with integrated AI units (Fig. 14). An example of the former is the Raspberry Pi AI HAT+, while a notable example of the latter is the ArduCam series, specifically the SONY IMX500 model. The IMX500 is equipped with an integrated AI processor capable of performing preliminary image processing and inference directly on the sensor.

These technologies are particularly well-suited for edge computing applications utilizing lightweight neural networks. Leveraging both independently acquired data and resources from the CREDO initiative, plans are underway to training a neural network based on the MobileNet architecture. The hardware integration of a Raspberry Pi controller with the IMX500 camera, combined with an implemented classification model, enables substantial data reduction directly at the sensor level, significantly decreasing the computational load on the controller's processor. This efficiency suggests that even the controllers with lower computational capabilities, such as the Raspberry Pi 3 or Pi Zero, could effectively support this type of camera for such applications.

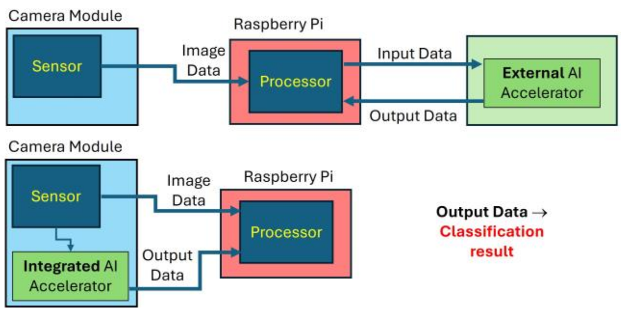


Fig. 14. AI implementation models in vision sensor

**Selected examples of analysis of extracted data**

In the field of cosmic-ray research, data acquired from CMOS matrix sensors hold significant interest for multiple applications. Beyond the widely studied classification of particle traces, these data facilitate detailed investigations into metrological properties, encompassing both small- and large-scale geometric features of traces in 2D and 3D. The resolution of recorded traces is influenced by the pixel size of the sensors used in vision detectors, as evidenced by statistical analyses of cropped image series obtained from the IMX296 and HawkEye sensors (Fig. 15).

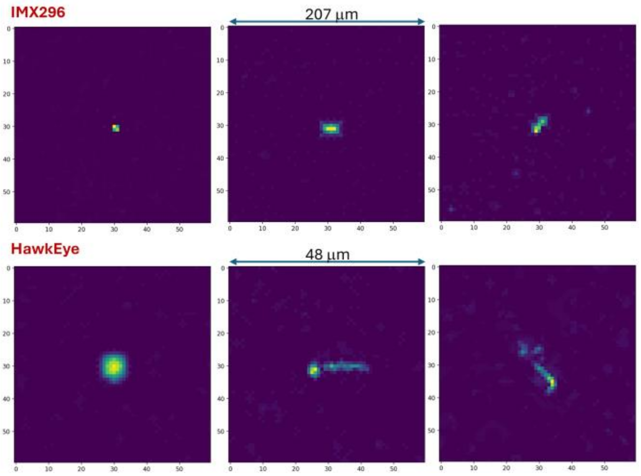


Fig. 15. Typical differences in trace detail in images from sensors with different pixel sizes

The detailed structure of traces captured in images provides opportunities to extract supplementary information, such as pixel brightness variations and the dimensions of characteristic features. These data are valuable for interpreting the origins of the observed traces (Fig. 16)

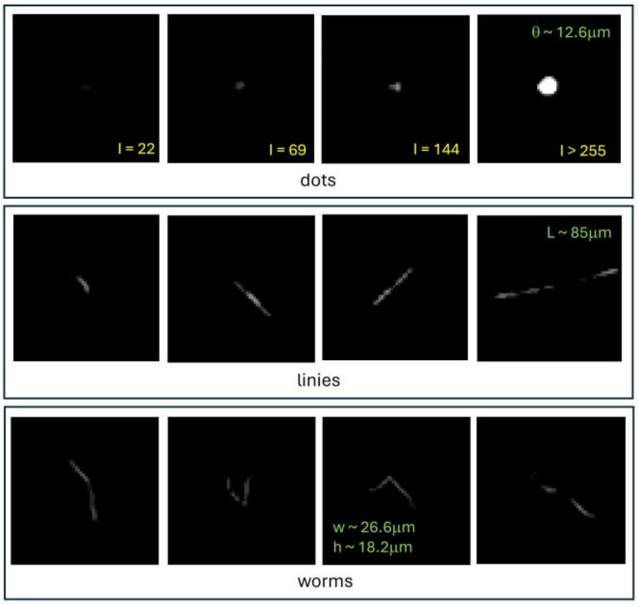


Fig. 16. Examples of traces recorded with the OV5647 sensor.

Particularly noteworthy are the rare occurrences of multiple traces within a single image (Fig. 17).

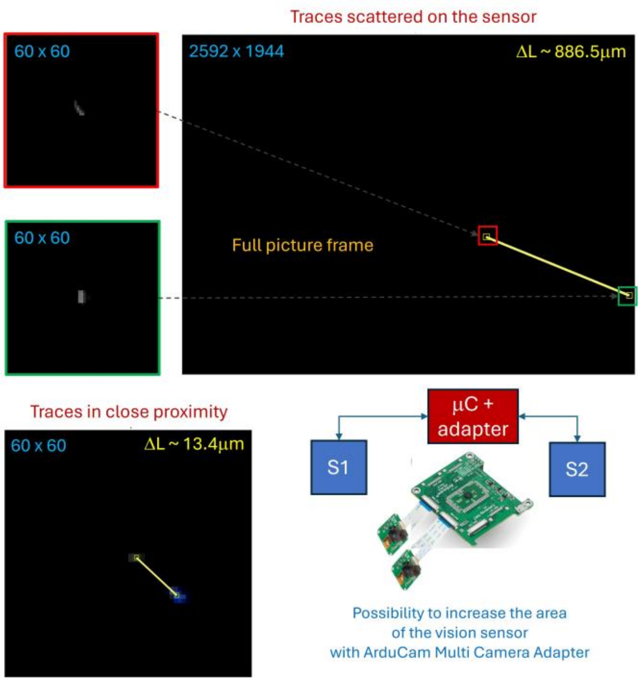


Fig. 17. Examples of multiple traces and sensor configurations with a dedicated dual-sensor support adapter.

Given the small physical size of the sensors and the low frequency of such phenomena relative to the image acquisition times (approximately 0.1–1 s), these multiple traces may suggest a common origin from the same atmospheric air shower. Similarly, the sparse occurrence of traces distributed across larger sensor areas highlights the need for detection systems with increased surface coverage.

In the absence of large-scale sensors, a viable alternative to the ArduCam series could be the use of specialized adapters that enable the synchronized operation of multiple smaller sensors. This approach offers an efficient means to expand the effective detection area while mitigating the limitations associated with the use of individual large-format sensors.

An additional valuable piece of information, particularly for characterizing the structure of an atmospheric air shower, is the direction of the particle’s "motion/arrival," which can be inferred from the analysis of linear traces. In a two-dimensional approach (azimuth determination), this is accomplished by analyzing the orientation of the trace on the sensor in conjunction with the sensor's alignment relative to geographic north, a metadata attribute associated with the sensor and stored in the database. A three-dimensional analysis becomes possible using a layered detector configuration, assuming simultaneous trace registration on two sensors. Both approaches are illustrated in Fig. 18.

Simultaneous trace detection on two sensors not only provides temporal synchronization for muon acquisition (enabling particle type identification) but also facilitates the determination of the muon’s directional vector within a three-dimensional coordinate system by analyzing the geometric relationship between the traces on both sensors. Ongoing hardware and analytical efforts to develop such vision sensor configurations featuring an adapter with a Raspberry Pi 4 controller and synchronized operation of two cameras using a Raspberry Pi 5 are currently in the preliminary research phase.

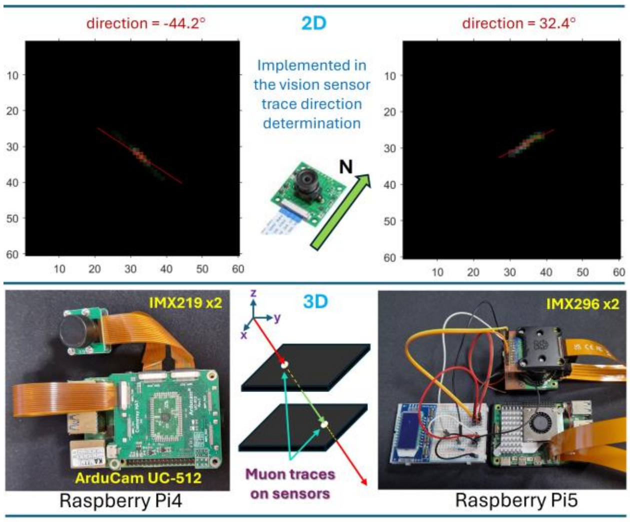


Fig. 18. Variant solutions for trace directionality analysis in the form of two- and three-dimensional information.

### Complementary solutions for the IoT system

In order to improve the management and monitoring of such a distributed IoT information system, a preliminary software version for a mobile device (Android smartphone) has also been developed. Application is designed to display information about recently detected cosmic rays, as well as to configure sensors by updating their software, turning them on or off, and adjusting their settings. The selected screenshots are presented in the Figure 19 for more information, see GitHub repository [23].

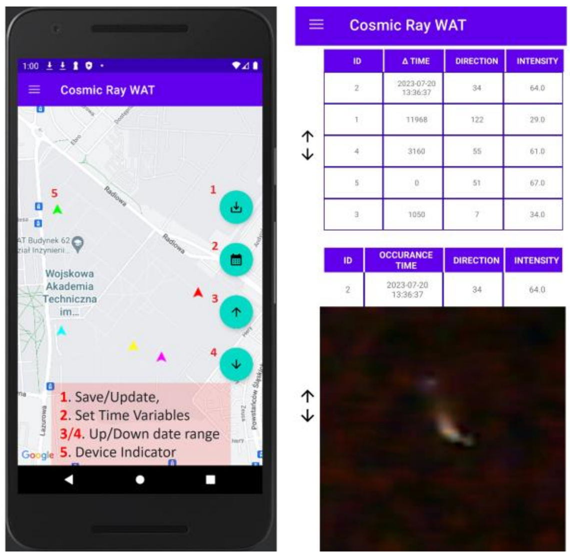


Fig. 19. Test application for monitoring and configuration of vision sensors for Android device

To streamline the testing of algorithms designed for the analysis of images containing cosmic-ray traces, a Python application was developed. This application provides functionality for browsing periodically retrieved resources from the CREDO database (Fig. 20) and supports the import of archived images encoded as Base64 ASCII strings.

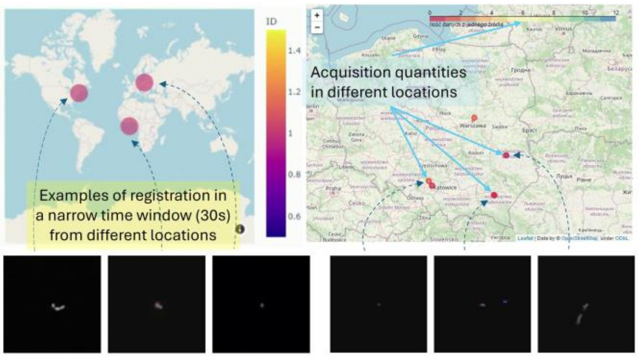


Fig. 20. CREDO data viewer from the selected time window.

**Summary**

The concept of a local cosmic-ray monitoring system on the WAT campus exemplifies the scientific evolution of a citizen science initiative, as represented by CREDO. The proposed IoT system emphasizes the integration of edge computing with data acquired through diverse techniques, such as precise timing measurements from muon sensors. This approach addresses certain limitations inherent in systems relying solely on vision sensors.

The solutions presented primarily focus on characterizing efficient vision sensors. The experimental results clearly demonstrate a significant performance improvement when using the Raspberry Pi 5 controller. This improvement is attributed to the ability to achieve near 100% utilization of sensor operation time while maintaining real-time processing of each captured frame. The enhanced computational capabilities of the Pi 5 also enable the implementation of advanced algorithms, including lowering detection thresholds for cosmic rays and introducing sophisticated trace classification techniques.

Among the various tested ArduCam series sensors, several exhibited low average noise levels and relatively few anomalous pixels, making them strong candidates for vision sensor applications. The Pi 5 successfully supported the HawkEye sensor, which, despite a stable operational frequency of 2 Hz, offers the highest level of detail in recorded traces. Higher operational frequencies were achieved with the IMX477 sensor, which, although providing slightly lower spatial resolution, enables lower detection thresholds and potentially increases the number of detected events within the same time frame. Furthermore, the IMX296 sensor, featuring a global shutter and synchronized operation capability, is particularly suitable for muon detection and determining their 3D directional vectors in a dual-layer sensor configuration.

The conceptual framework of the proposed IoT system has also inspired the active participation of young researchers - students, graduates, and doctoral candidates encouraging them to explore innovative solutions across hardware, algorithmic, and system-level domains. Their involvement in the development of the solutions outlined in this article highlights the value of engaging contributors outside the core scientific community, reaffirming the importance and potential of citizen science initiatives as a model for future research ventures.

***Authors**: dr hab. inż. Marek Piszczek, profesor WAT, Wojskowa Akademia Techniczna, Instytut Optoelektroniki, ul. gen. S. Kaliskiego 2, 00-908 Warszawa, E-mail: marek.piszczek@wat.edu.pl;*
*mgr inż. Aleksandra Kucharczyk-Drab, Wojskowa Akademia Techniczna, Instytut Optoelektroniki, ul. gen. S. Kaliskiego 2, 00-908 Warszawa, E-mail: aleksandra.kucharczyk@wat.edu.pl;*
*Adam Piszczek, Wojskowa Akademia Techniczna, ul. gen. S. Kaliskiego 2, 00-908 Warszawa, E-mail: adam314pi@gmail.com*

REFERENCES

[1] Auger. P, Ehrenfest.,R, Maze., J, Daudin., Freon Robley., A, Extensive cosmic ray showers, Reviews of Modern Physics, 11(1939), 288-291
[2] Greisen K, Cosmic Ray Showers, Annual Review of Nuclear and Particle Science 10(1960), 63-108
[3] Zavrtanik D., The Pierre Auger observatory, Nuclear Physics B - Proceedings Supplements, 85(2000), 324-331
[4] Cao Z., Chen M., Chen S., et.al, Introduction to Large High Altitude Air Shower Observatory (LHAASO), Acta Astronomica Sinica 60(2019), 19
[5] AbuZayyad T., Aida R., Allen M., et al., The surface detector array of the Telescope Array experiment, Nuclear Instruments and Methods in Physics Research Section A: Accelerators, Spectrometers, Detectors and Associated Equipment 689(2012), 87-97
[6] Abbasi R., Allen M., Arimura R., et all, An extremely energetic cosmic ray observed by a surface detector array, Science, 382(2023), 903-907
[7] Homola P., Beznosko D.; Bhatta G.; Bibrzycki Ł.; et al. Cosmic-Ray Extremely Distributed Observatory. Symmetry 12(2020)
[8] Bykov A., Aharonian F., Krassilchtchikov A., et al. Cherenkov gamma-ray telescopes: Past, present, future. The ALEGRO project, Tech. Phys. 62(2017), 819–836
[9] Watson A., The discovery of Cherenkov radiation and its use in the detection of extensive air showers, Nuclear Physics B - Proceedings Supplements, 212-213(2011), 13-19
[10] Albert A., Alfaro R., C. Alvarez C., *et al.,* Performance of the HAWC Observatory and TeV Gamma-Ray Measurements of the Crab Nebula with Improved Extensive Air Shower Reconstruction Algorithms, *The Astrophysical Journal* 972(2024), No. 2
[11] M. Abbrescia et al., First detection of extensive air shower with the EEE experiment, 2009 *IEEE Nuclear Science Symposium Conference Record (NSS/MIC),* Orlando, FL, USA, 2009, 439-443
[12] Adriani O., Barbarino GC., Bazilevskaya GA., *Italian Physical Society*, 10(2017), 473-522
[13] Abe K., Fuke H., Haino S., et.al, The results from BESS-Polar experiment, Advances in Space Research 60(2017), No. 4, 806-814
[14] Vandenbroucke J., Runze Li., Pizzuto A., Citizen science with the Distributed Electronic Cosmic-ray Observatory (DECO), *244th Meeting of the American Astronomical Society*, 56(2024), No. 7
[15] Bibrzycki, Ł.; Burakowski, D.; Homola, P.; et al. Towards A Global Cosmic Ray Sensor Network: CREDO Detector as the First Open-Source Mobile Application Enabling Detection of Penetrating Radiation. Symmetry 12(2020), No. 11
[16] http://cosmicpi.org/
[17] Axani S., Frankiewicz K., Conrad J., The CosmicWatch Desktop Muon Detector: a self-contained, pocket sized particle detector, Journal of Instrumentation, 13(2018), No. 03
[18] Meuris A., Nagazawa K., Kuvvetli I., Caroli E., Cd(Zn)Te Detectors for Hard X-Ray and Gamma-Ray Astronomy, *Handbook of X-ray and Gamma-ray Astrophysics, Springer, Singapore* 2023, 1-36
[19] LIU Z., Measurement of Cosmic-Ray Magnesium and Aluminum Fluxes with the Alpha Magnetic Spectrometer on the International Space Station 2021, Doctoral Thesis, 21-25
[20] Del Sordo S, Abbene L, Caroli E, Mancini AM, Zappettini A, Ubertini P. Progress in the Development of CdTe and CdZnTe Semiconductor Radiation Detectors for Astrophysical and Medical Applications. Sensors 9(2009); No. 5
[21] Piekarczyk M, Hachaj T., On the Search for Potentially Anomalous Traces of Cosmic Ray Particles in Images Acquired by Cmos Detectors for a Continuous Stream of Emerging Observational Data, Sensors 24(2024), No. 6
[22] Hachaj T, Bibrzycki Ł, Piekarczyk M. Recognition of Cosmic Ray Images Obtained from CMOS Sensors Used in Mobile Phones by Approximation of Uncertain Class Assignment with Deep Convolutional Neural Network, Sensors 21(2021), No. 6,
[23] https://github.com/Adam-The-Programmer/Cosmic-Ray-WAT-Public